Available online at www.sciencedirect.com
SCIENCE DIRECT®
Journal of Magnetic Resonance 169 (2004) 313–322
JMR Journal of Magnetic Resonance
www.elsevier.com/locate/jmr

Restricted diffusion within a single pore

M.E. Hayden,* G. Archibald, K.M. Gilbert, and C. Lei

Department of Physics, Simon Fraser University, Burnaby, BC, Canada V5A 1S6

Received 17 March 2004; revised 5 May 2004
Available online 11 June 2004

Abstract

The time-dependent diffusion of ^{3}He atoms perpendicular to the axis of a single macroscopically large cylindrical pore is studied using a steady (or constant) gradient-recalled echo sequence. Measurements of the effective ^{3}He diffusion coefficient extending from the free-diffusion regime to the motionally averaged regime are presented, and are well-described by analytic solutions to the Bloch–Torrey equation based on the gaussian phase approximation. Our data yield the value 0.140(6) m^2/s for the self diffusion coefficient of ^{3}He at a temperature of 296 K and a pressure of 1.00 Torr. Adaptations of these methods should enable the study of complex pore geometries as model systems.

PACS: 76.60.−k; 51.20.+d

Keywords: Low-field NMR; ^{3}He; Hyperpolarized gas; Restricted diffusion; Apparent diffusion coefficient; Gaussian phase approximation; Cylindrical pore

1. Introduction

Hahn's 1950 treatment of the spin echo problem [1] established the framework for an entire class of experiments that provide robust and versatile probes of diffusion phenomena [2–5]. Modern applications range from non-invasive measurements of the diffusivity of water and metabolites in tissues [6] and gases in lungs [7] to the characterization of transport phenomena in hydrocarbon-bearing reservoir rocks and other porous media [8–10]. A significant number of these applications involve 'bounded' or 'restricted' diffusion, in which random translational motions are strongly influenced (impeded) by physical or structural barriers [11]. Accurate determinations of pore morphology from experiments that probe restricted diffusion ultimately rely on the precision of underlying theories and the assumptions upon which they are based. It is thus noteworthy that data from systematic studies of NMR-detected restricted diffusion within well-defined (i.e., model) geometries are sparse.

Although real pore systems tend to be polydisperse and polymorphic, it is both instructive and important to study realizations of simple one-, two-, and three-dimensional restrictions: parallel plates of infinite extent, cylinders of infinite length, and spherical volumes, respectively. A variety of NMR-based techniques have previously been used to study the diffusion of liquids and dense gases between arrays of closely spaced parallel plates [4,12–15], within arrays of small rectangular channels [16], within thin films ('slabs') of fluid confined by parallel plates [17,18], and within long narrow cylindrical tubes [19]. These experiments employ liquids and dense gases diffusing in pores with characteristic dimensions of order 100 μm, and typically probe a range of diffusion length scales that span the unrestricted- and restricted-diffusion limits.

Here, we report the results of a study that probes the diffusive motion of a *low pressure* gas confined to a single finite-length cylindrical pore with non-relaxing walls and dimensions of order several centimeters. By directing NMR field gradients perpendicular to the axis of the cylinder our experiment probes random translational motions that are restricted in two dimensions; the end-walls of the cylinder effectively act

* Corresponding author. Fax: +1-604-291-3592.
E-mail address: mhayden@sfu.ca (M.E. Hayden).

1090-7807/$ - see front matter © 2004 Elsevier Inc. All rights reserved.
doi:10.1016/j.jmr.2004.05.002

as perfect reflecting boundaries and allow us to treat the cylinder as if it were infinite in extent. By varying the magnitude of these field gradients and their time of application we probe a range of motions that extend from the free-diffusion to the motionally averaged regimes.

A clear advantage to working with macroscopically large model pores rather than microscopic systems is the potential for studying diffusion in complex yet well-defined geometries. One of our goals here is thus to demonstrate that a reasonable range of parameter space can be accessed with the methods we describe. At the same time we have taken the opportunity to perform an experiment that explores a range of diffusion length scales that has not been previously examined for cylindrical geometries. In this context we observe excellent agreement between our data and an oft-cited yet only indirectly tested theoretical model based on the gaussian phase approximation [20].

Finally, we employ what is in effect a constant field gradient (i.e., Carr–Purcell based [2]) approach to the measurement of time-dependent diffusion coefficients. While this is a departure from the methodology used for the majority of modern NMR-based measurements of diffusion, which derive from the short gradient-pulse methods of Stejskal and Tanner [4], it is not intrinsic to the experiment we describe. One could view our experiments as encompassing the extreme limit of a finite-width pulsed-gradient experiment in which the pulse width is equal to the diffusion time. This is a limit that is of interest in its own right in the context of trying to understand the breakdown of the short gradient pulse approximation [18,21–23]. We begin by outlining a number of issues and equations that are relevant to NMR-based studies of restricted diffusion in the constant gradient limit.

2. Background

Unrestricted diffusion in a constant and uniform magnetic field gradient of amplitude g leads to an attenuation of the Hahn spin-echo amplitude at time 2τ that is given by[1]

$$\frac{M(g,\tau)}{M(0,\tau)} = \exp\left[-\frac{2}{3}D_0\gamma^2 g^2 \tau^3\right], \tag{1}$$

where M is the average transverse magnetization density, γ is the gyromagnetic ratio of the diffusing spins, and D_0 is the free or unrestricted diffusion coefficient. It is often argued that Eq. (1) remains valid within restricted geometries, as long as the characteristic length scale for diffusion $\ell_d = \sqrt{D_0\tau}$ along the field gradient during the measurement period τ remains small compared to the characteristic size ℓ_s of the confining pore or structure. Some care must be exercised in the selection of an absolute value for ℓ_s, particularly if comparisons between experiments involving restrictions in different dimensions are to be made. To first approximation one expects ℓ_s to represent an appropriately averaged geometric length scale related to the surface area-to-volume ratio or the mean curvature of the pore space, as discussed by de Swiet and Sen [30]. This is an issue that we revisit in the context of our data analysis in Section 4.

As early as 1962 Woessner [24] noted that increasing the measurement time, such that ℓ_d becomes comparable to or greater than ℓ_s, leads to an effective suppression of the diffusion coefficient. Shortly thereafter, Wayne and Cotts [12] published the first systematic investigation of this effect in a well-defined geometry. They used constant gradient spin-echo techniques to study the diffusion of high-pressure methane gas confined between a series of closely spaced parallel plates. When the field gradient was directed normal to the plates they observed a decrease in the echo attenuation factor (Eq. (1)) that was consistent with a numerical solution to an approximation of the Bloch equations as modified by Torrey [25,26] to include a diffusion term. They recognized this *apparent* suppression of the diffusion coefficient as being due to the effects of motional averaging, and observed that once spins were allowed to diffuse distances large compared to pore dimensions (i.e., $\ell_d \gg \ell_s$) the echo-attenuation factor becomes a simple exponential decay. By considering the spectral density of field fluctuations encountered by diffusing spins Wayne and Cotts demonstrated that in the motionally averaged limit

$$\frac{M(g,\tau)}{M(0,\tau)} = \exp\left[-\frac{\beta\gamma^2 g^2 \ell_s^4 2\tau}{D_0}\right], \tag{2}$$

where $\beta = \beta_1 = 2/15$ and $\ell_s = a/2$ for diffusion perpendicular to a series of infinite reflecting planes separated by a distance a.[2]

Motivated by Cotts, Robertson [27] undertook the first detailed theoretical treatment of the restricted diffusion problem. His approximate analytic solution to the Bloch–Torrey equations led to the expression

[1] Echo-attenuation factors suitable for application to variations of the basic Hahn echo experiment can be found in textbooks on magnetic resonance [9,11]. The work reported here makes use of a constant gradient-recalled echo sequence for which Eq. (1) is appropriate.

[2] The subscript '1' associated with the parameter β indicates that the value 2/15 is appropriate for a one-dimensional restriction. Two- and three-dimensional restrictions are discussed later.

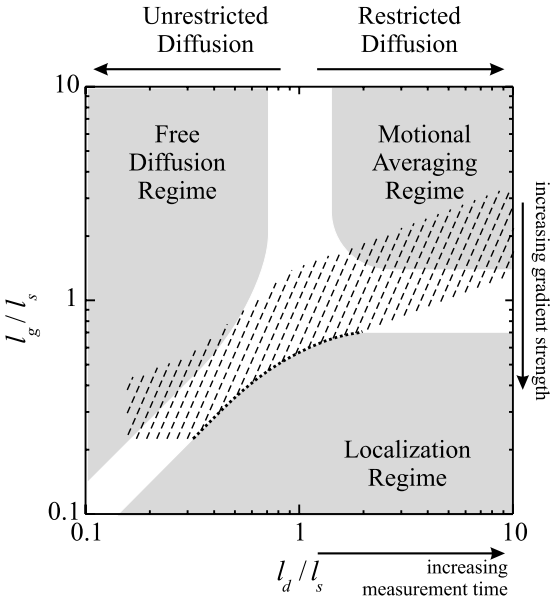

Fig. 1. Spin-echo attenuation factors exhibit three limiting types of behavior as summarized in this figure, which has been adapted from reference [14]. The parameters ℓ_s, ℓ_d, and ℓ_g correspond to characteristic structural, diffusion, and dephasing length scales as described in the text. Boundaries between the various regimes are not sharp, and have not been fully characterized [28]. The hatched region indicates the range of parameter space explored as part of the present investigation, while the dotted line represents our estimate of the boundary between the intermediate and localization regimes as described in Section 3.

$$\frac{M(g,\tau)}{M(0,\tau)} = \exp\left[-\frac{8\gamma^2 g^2 a^4}{\pi^6 D_0}\sum_{n=0}^{\infty}\frac{1}{(2n+1)^6}\left(2\tau - \frac{3-4\exp\left[-D_0(2n+1)^2\pi^2\tau/a^2\right]+\exp\left[-D_0(2n+1)^2\pi^2 2\tau/a^2\right]}{D_0(2n+1)^2\pi^2/a^2}\right)\right] \quad (3)$$

for the infinite parallel reflecting-plane geometry. This result is indistinguishable from the numerical calculation that was performed by Wayne and Cotts. It reduces to Eq. (1) for $\ell_d \ll \ell_s$ and to Eq. (2) for $\ell_d \gg \ell_s$.

Underlying Robertson's derivation of Eq. (3) is an important set of constraints related to the strength of the applied field gradients.[3] These constraints are conveniently described in terms of the dephasing length $\ell_g = (D_0/\gamma g)^{\frac{1}{3}}$ characteristic of the average distance that a spin must diffuse in order to dephase by 2π radians with respect to a stationary spin. Hürlimann et al. [14] provide an excellent discussion of the interplay that occurs between the three length scales that are relevant to this problem: ℓ_s, ℓ_d, and ℓ_g. Fig. 1 summarizes the dependence of spin-echo attenuation factors on the relative sizes of these various length scales.

Robertson noted that Eq. (3) should be rigorously valid for short measurement times such that $\ell_d \ll \ell_s$ and $\ell_d \ll \ell_g$. In principle this corresponds to the free-diffusion regime identified by Hürlimann et al. [14] and shown in Fig. 1 (i.e., the regime in which ℓ_d is the smallest length scale). In practical terms, it should be noted that this is the limit in which Eq. (3) reduces to Eq. (1), which can be written in the form

$$\frac{M(g,\tau)}{M(0,\tau)} = \exp\left[-\frac{2}{3}\left(\frac{\ell_d}{\ell_g}\right)^6\right], \quad (4)$$

and thus ℓ_g cannot be made substantially larger than ℓ_d without effectively destroying the experimental signature of the diffusion process. In other words, the 'free diffusion' regime identified in Fig. 1 is largely inaccessible to experiments that rely on constant gradient techniques; instead these experiments probe the (poorly understood) intermediate regime between the free-diffusion and localization regimes. Robertson also concluded that Eq. (3) should be valid for arbitrary times as long as $\ell_g > \ell_s$ (the motional averaging regime, in which ℓ_s is the smallest length scale in the problem), although he was unable to quantify the exact nature of the breakdown of this constraint in the vicinity of $\ell_g \sim \ell_s$. Wayne and Cotts' numerical solution of the Bloch equations and their derivation of Eq. (2) were subject to the same constraint.

In 1973, Neuman [20] reformulated the restricted diffusion problem in terms of the random accumulation of phase [29]. With the assumption that the distribution of phase changes is gaussian he was able to reproduce Eq. (3). The validity of this assumption is difficult to assess for complex geometries.[4] However, it is clear that when ℓ_g is the smallest length scale in the problem the phase distribution deviates strongly from a gaussian and the spin echo envelope becomes an exponential with a rate that is proportional to $g^{2/3}$ [30,33] rather than g^2. Hürlimann et al. [14] refer to this as the localization regime, and were the first to provide a clear experimental demonstration of its existence.

Neuman went on to derive expressions analogous to Eq. (3) for spins confined to cylindrical and spherical volumes with perfectly reflecting boundaries [20]. For a constant and uniform magnetic field gradient directed perpendic-

[3] Wayne and Cotts invoked the same approximation in carrying out their numerical solution of the Bloch equations.

[4] It is expected to be rigorously valid for the motionally averaged and free diffusion regimes [20,30], but not necessarily valid in the intermediate regime. Further discussion of this issue can be found in references [31] and [32].

ular to the axis of a confining cylinder of radius R the attenuation of the Hahn spin echo amplitude is given by

$$\frac{M(g,\tau)}{M(0,\tau)} = \exp\left[-\frac{2\gamma^2 g^2}{D_0} \sum_{n=1}^{\infty} \frac{\alpha_n^{-4}}{\alpha_n^2 R^2 - 1} \times \left(2\tau - \frac{3 - 4\exp\left(-\alpha_n^2 D_0 \tau\right) + \exp\left(-\alpha_n^2 D_0 2\tau\right)}{\alpha_n^2 D_0} \right) \right], \tag{5}$$

where α_n is the nth root of $J_1'(\alpha_n R)$, while for a sphere of radius R the corresponding expression is

$$\frac{M(g,\tau)}{M(0,\tau)} = \exp\left[-\frac{2\gamma^2 g^2}{D_0} \sum_{n=1}^{\infty} \frac{\kappa_n^{-4}}{\kappa_n^2 R^2 - 2} \times \left(2\tau - \frac{3 - 4\exp\left(-\kappa_n^2 D_0 \tau\right) + \exp\left(\kappa_n^2 D_0 2\tau\right)}{\kappa_n^2 D_0} \right) \right], \tag{6}$$

where κ_n is the nth root of $\kappa_n R J_{3/2}'(\kappa_n R) - \frac{1}{2} J_{3/2}(\kappa_n R) = 0$. Eqs. (5) and (6) both reduce to Eq. (1) in the free diffusion regime and to Eq. (2) in the motionally averaged regime, with $\beta = \beta_2 = 7/96$ for the cylinder,[5] $\beta = \beta_3 = 8/175$ for the sphere,[6] and $\ell_s = R$ in both cases.[7]

Eqs. (3), (5), and (6) define the canonical forms of the Hahn spin echo amplitude for simple restricted diffusion in one, two and three dimensions[8] as long as the localization regime is avoided. Of these, only Eq. (3) (corresponding to the slab, or one-dimensional geometry) has been directly tested with constant gradient techniques over a continuous range of diffusion length scales spanning the unrestricted- and restricted-diffusion limits [12]. The work of Bohler and McGregor [36,37] with cylindrical cells and the work of Barbé et al. [38] and later Cates et al. [39] with spherical cells effectively test the motionally averaged limits of Eqs. (5) and (6), respectively, but do not probe the unrestricted-diffusion limit. Our experiments with low-pressure ^{3}He gas provide a direct test of Eq. (5) (cylindrical, or prototypical two-dimensional restriction) that extend from the free-diffusion regime to the motionally averaged regime, all-the-while avoiding the problematic localization regime. The latter point is significant as it is now clear that Wayne and Cott's well-known study of restricted diffusion was at least partially performed in the localization regime [14].

Before proceeding, we note that a convenient way of describing data from restricted diffusion experiments is to introduce an effective *time-dependent* diffusion coefficient D_{eff}. Following Wayne and Cotts, Eqs. (3), (5), and (6) can be formally expressed in terms of Eq. (1) by defining

$$D_{\mathrm{eff}} = \frac{12a^4}{\pi^6 D_0 \tau^3} \sum_{n=0}^{\infty} \frac{1}{(2n+1)^6} \left(2\tau - \frac{3 - 4\exp\left[-D_0 (2n+1)^2 \pi^2 \tau / a^2 \right] + \exp\left[-D_0 (2n+1)^2 \pi^2 2\tau / a^2 \right]}{D_0 (2n+1)^2 \pi^2 / a^2} \right) \tag{8}$$

for diffusion normal to infinite reflecting planes separated by a distance a,

$$D_{\mathrm{eff}} = \frac{3}{D_0 \tau^3} \sum_{n=1}^{\infty} \frac{\alpha_n^{-4}}{\alpha_n^2 R^2 - 1} \left(2\tau - \frac{3 - 4\exp\left(-\alpha_n^2 D_0 \tau\right) + \exp\left(-\alpha_n^2 D_0 2\tau\right)}{\alpha_n^2 D_0} \right) \tag{9}$$

for diffusion perpendicular to the axis of an infinite reflecting cylinder of radius R, and

$$D_{\mathrm{eff}} = \frac{3}{D_0 \tau^3} \sum_{n=1}^{\infty} \frac{\kappa_n^{-4}}{\kappa_n^2 R^2 - 2} \left(2\tau - \frac{3 - 4\exp\left(-\kappa_n^2 D_0 \tau\right) + \exp\left(\kappa_n^2 D_0 2\tau\right)}{\kappa_n^2 D_0} \right) \tag{10}$$

for diffusion within a reflecting sphere of radius R. One thus expects to observe

$$\frac{M(g,\tau)}{M(0,\tau)} = \exp\left[-\frac{2}{3} D_{\mathrm{eff}} \gamma^2 g^2 \tau^3 \right] \tag{11}$$

for both short and long diffusion times.

[5] Neuman's oft-cited manuscript contains a typographical error that does not appear to have been previously documented. We have repeated his calculations and find that numerical prefactor 7/296 appearing in Eq. (28) of reference [20] should read 7/96.

[6] Further discussion regarding the nature of the irreversible loss of spin coherence due to diffusion in a spherical container can be found in references [34] and [35].

[7] McGregor later used techniques similar to those first employed by Wayne and Cotts to derive expressions for the transverse relaxation time T_2 of a gas of polarized ^{3}He atoms diffusing in a magnetic field gradient [37]. His results, which are pertinent to the motional averaging regime, are effectively identical to those presented by Neuman as far as the irreversible loss of coherence due to translational diffusion is concerned.

[8] Under more general conditions, where spins are free to diffuse within an arbitrary bounded (although not necessarily connected) pore space with reflecting boundaries the Hahn spin-echo amplitude is given by

$$\frac{M(g,\tau)}{M(0,\tau)} = \exp\left[-\frac{2}{3} \left(\frac{\ell_d}{\ell_g} \right)^6 \left(1 - \frac{3\alpha}{d} \frac{S}{V} \ell_d + \vartheta\left(\ell_d^2\right) \right) + \vartheta\left(\frac{\ell_d^{13}}{\ell_g^{12}} \frac{S}{V} \right) \right], \tag{7}$$

where $\alpha = 32(2\sqrt{2} - 1)/105\sqrt{\pi} \approx 0.3144 \ldots$, S/V is the pore space surface-area-to-volume ratio, and d is the number of dimensions in which the motion is restricted. Eq. (7) was first derived by Helmer et al. [13] using the methods of de Swiet and Sen [30] to expand around the gaussian phase approximation at short echo times; it is only valid outside of the localization regime.

3. Experimental

The cells used in this work were made entirely from borosilicate glass [40], and were fabricated by oven-sealing the two ends of a 4.84(1) cm ID tube with matching optical flats. The misalignment of the endwalls with respect to the axis of the cylinder was typically no greater than 0.2°. A 6 mm ID tube attached to the cylindrical wall of each cell provides a means for evacuating and filling the cell. After fabrication, the interior of each cell was etched with hydrofluoric acid and thoroughly rinsed. The cell was then oven-annealed in air for 20 min at 560 °C. At this point the cells were attached to a glass manifold[9] and evacuated to pressures below 10^{-6} Torr while being heated to temperatures of order 250 °C for time periods of several days. The final step in the cleaning procedure involved filling the cell with approximately 1.5 Torr of 99.9999 mol % ^{4}He and igniting an intense rf discharge by coupling approximately 200 W of microwave power from a commercial microwave oven into the cell. After several minutes, and before the softening temperature of the glass is reached, the contents of the cell are evacuated and the procedure repeated. Contaminants within the cell were detected and monitored by observing the optical emission spectrum of the gas using a CCD-based optical spectrometer.[10] Typically, we observe a substantial decrease in the relative intensity of spectral features *not* associated with helium over the first 5–10 iterations of this discharge-cleaning procedure. Approximately, 15 iterations were used in the preparation of the particular cells used in the present work. The final stage in the preparation of each experimental cell involved filling them with ^{3}He gas[11] to a pressure of 1 Torr, and then flame-sealing and annealing the fill-tube, leaving a short stub comprising less than 0.1% of the total volume. We have found that cells prepared in this manner consistently yield longitudinal nuclear relaxation times T_1 in excess of 140 min at room temperature, increasing to more than 360 min at −100 °C. The mechanism responsible for this residual decay is associated with the diffusion of ^{3}He atoms into the glass matrix [43].

NMR measurements were performed using a custom-designed whole-body ultra-low-field magnetic resonance (MR) imaging system that operates at fields as high as 10 mT. The particular work described in this manuscript was carried out at a ^{3}He Larmor frequency of 19.8 kHz, corresponding to a static magnetic field of 611 μT. Pulsed field-gradients with maximum amplitudes of 13 mT/m were available, although no gradients larger than ~3 mT/m were applied as part of this investigation. A typical experimental sequence involved placing the cell at the isocentre of the magnet with the axis of the cell aligned to within 2° of the field, and then using metastability-exchange optical pumping techniques [44] to induce high nuclear spin polarizations in the low pressure gas.[12] MR pulse sequences were then initiated by applying a $\pi/2$ tipping pulse and acquiring the resulting free induction decay (FID).[13] All FID data were fit to complex exponentially damped sinusoids in order to extract signal amplitudes and damping rates.

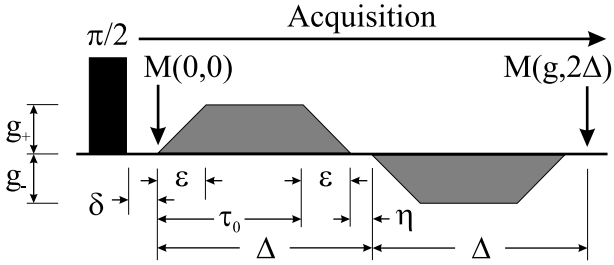

Fig. 2. Pulse sequence (not to scale): a symmetric bipolar field gradient is used to induce an abrupt attenuation of an FID. The attenuation factor $M(g,2\Delta)/M(0,2\Delta)$ can be related to an effective diffusion coefficient as outlined in Section 2. In the absence of applied field gradients, T_2^* is much longer than any of the timescales referenced here. This is a constant gradient approach to the measurement of diffusion coefficients in the sense that field gradients are applied throughout the entire period of time that spins are allowed to diffuse.

After a homogenization period δ of order 100 ms that is intended to eradicate spatial variations in the initial magnitude of the transverse magnetization, a bipolar field gradient is applied perpendicular to the axis of the cell. In effect this is a gradient-recalled echo sequence (see Fig. 2). It leads to an abrupt attenuation of the detected signal that is characterized by determining the ratio of the FID magnitude immediately before and after the gradient pulses. Small corrections to this ratio are made using measured values of T_2^* to account for the

[9] Valves and joints in this system were lubricated with Apiezon H vacuum grease [41].

[10] Typically, we monitor the spectral range from 300 to 1100 nm; however, we generally find that the range from 500 to 650 nm is sufficient to characterize the contamination level within the cell.

[11] The primary contaminant of concern from the point of view of nuclear relaxation studies is molecular oxygen [42], which is paramagnetic. The nominal O_2 concentration in the ^{3}He used in this work was 1 ppm.

[12] Specifically, a 10 MHz electrodeless discharge was used to populate the 2^3S state of the ^{3}He atoms while circularly polarized 1083 nm radiation generated by a laser diode was used to optically pump the 2^3S–2^3P transition. Nuclear polarization levels of order 20% were generated on a timescale of order 1 min using approximately 20 mW of optical radiation, after which time the discharge was extinguished.

[13] The receive coils used in this application represent a variation of the design described by Purcell [45]. Four identical, series-connected, coils were placed symmetrically about the axis of the cell. Two of the coils were arranged to form a coaxial pair while the other two formed a coplanar pair. The coils forming each pair were wound in the same sense, but the coaxial and coplanar pairs were counter-wound with respect to one another. This arrangement is tightly coupled to signals originating within the cell, but is virtually immune to disturbance from external sources.

influence of background field gradients. Corrections are also applied to the diffusion time to account for the finite slew rate of our gradient amplifiers. To first order these corrections are given by [13]

$$\tau = \tau_0 \left[1 + \frac{3(\epsilon + \eta)}{2\tau_0} - \frac{\epsilon^2}{4\tau_0^2} + \frac{\epsilon^3}{20\tau_0^3} \right]^{\frac{1}{3}}, \quad (12)$$

where the various symbols are defined in Fig. 2. Ramping times ϵ and interpulse delays η were individually determined for each pulse sequence, but were typically of order 20–100 μs and 250 μs, respectively.

Accurate absolute (static) calibrations of field gradients were performed by determining the Larmor frequency of a 3 cm-long ^{3}He-filled cell as a function of gradient current and cell position within the magnet. Dynamic field gradient amplitudes were subsequently checked and confirmed to be accurate by integrating the currents induced in a precision–balanced pair of coils wound in a gradiometric configuration and placed at appropriate locations within the magnet. Finally, gradient amplitudes were recorded for individual measurement sequences by monitoring currents produced by the gradient amplifiers. These amplitudes are reported as $\sqrt{(g_+^2 + g_-^2)/2}$, although positive and negative excursions (i.e., g_+ and g_-) were typically balanced at the level of 1% or better. A similar level of control was achieved in terms of the balance between the duration of the two field gradients.

4. Results and discussion

The timescale T_2^* for the decay of the precessing magnetization in our glass cells is limited by the diffusion of ^{3}He atoms in residual field gradients [37]. These gradients result from the intrinsic inhomogeneity of the magnet, as well as the presence of magnetic materials (such as light fixtures and structural steel) in the laboratory. Internal field gradients produced by susceptibility differences between the glass cell and the ^{3}He gas are completely negligible under the low-field conditions employed in our work. Ultimately, residual field gradients place a limit on the maximum period of time over which ^{3}He diffusion can be studied using the particular techniques we have described. Typically we use low-order shim coils to reduce residual gradients to the level of about 1 μT/m, beyond which point some care needs to be taken to ensure that magnetic materials (such as tools and furniture) located in the vicinity of the magnet remain stationary during an experimental sequence. In Fig. 3 we plot the magnitude of a typical FID acquired from a 3 cm-long ^{3}He-filled cell after shimming the magnetic field. The aspect ratio of this particular cell is such that it is predominately sensitive to transverse field gradients. Longitudinal components of residual gradients can be inferred by monitoring the Larmor frequency as a function of position as the cell is moved along the axis of the magnet. The fact that we have observed T_2^*'s more than an order of magnitude longer than pictured in this example simply by improving the field homogeneity provides assurance that the walls of our glass cells can be treated as if they are perfectly non-relaxing.

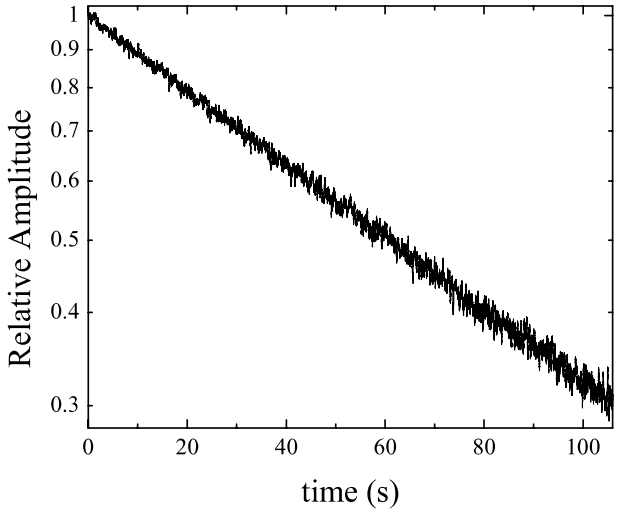

Fig. 3. The magnitude of an FID acquired from a 3 cm-long ^{3}He-filled cell. The decay pictured here is accurately exponential, and implies a residual field gradient of order 1 μT/m in the transverse direction (cf. Eq. (2)).

Measurements of gradient-induced FID attenuation factors were performed as a function of gradient strength for fixed diffusion times. The experimentally determined ratio $\ln[M(g, 2\Delta)/M(0, 2\Delta)]$ was then plotted as a function of $2\gamma^2 g^2 \tau^3/3$ to extract D_{eff} (cf. Eq. (11)). At high gradient amplitudes a clear departure from a linear relationship, consistent with the onset of the localization regime [14], could be observed; examples of such data are presented in reference [46] and the locus of points demarcating the observed change in behavior is shown in Fig. 1. The data presented in this manuscript were selected from the low gradient-amplitude limit, where a clear linear relationship between $\ln[M(g, 2\Delta)/M(0, 2\Delta)]$ and $2\gamma^2 g^2 \tau^3/3$ was evident.

In Fig. 4 we plot measured values of D_{eff} as a function of diffusion time τ for a 9 cm-long cylinder containing ^{3}He gas at a pressure of 1.00 Torr and a temperature of 296 K. The uncertainty in each point is of order the symbol size or smaller. Data acquired using a 3 cm-long cell rather than a 9 cm-long cell yield identical results within the limits of our experimental accuracy, reaffirming the assertion that the walls of our cells can be treated as ideal 'reflecting' boundaries. The circular symbols in Fig. 4 represent measurements performed with the cell oriented in the usual configuration as described in Section 3. The square symbol represents the result of a measurement that was made after rotating the cell by 90° so that its axis was parallel to the applied field

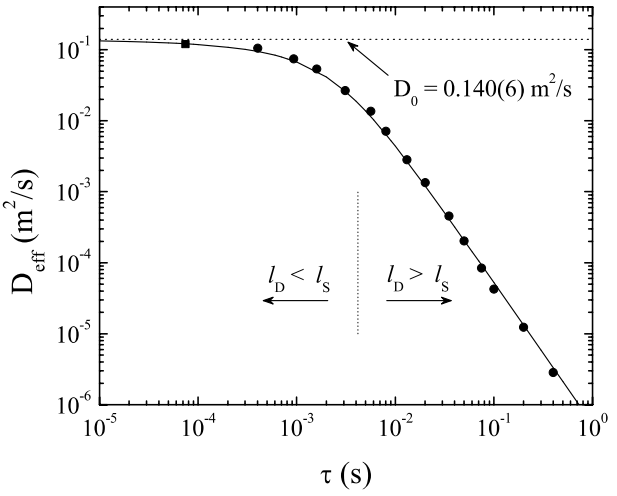

Fig. 4. Measured and calculated (Eq. (9)) values of the effective diffusion coefficient for low-pressure ^{3}He gas diffusing perpendicular to the axis of a single cylindrical pore. The range of characteristic length scales ℓ_s, ℓ_d, and ℓ_g explored in this measurement are shown in Fig. 1. The single data point marked by a square corresponds to a measurement made after rotating the cell by 90° so that its axis was parallel to the field gradient. This increases the relevant structural length scale ℓ_s effectively allowing us to probe time scales that are closer to the free diffusion limit. Further discussion of this measurement is given in the text.

gradient. Under these conditions, the roles of the flat- and cylindrical-walls of the cell are interchanged. That is, we expect the FID attenuation for this measurement to be described by the expression appropriate for infinite parallel plates. In effect, this manipulation provides a substantial increase in the relevant value of ℓ_s, allowing us to probe values of D_{eff} that are closer to the free diffusion limit. The abscissa for this point is an effective diffusion time, as discussed at the end of this Section.

The solid line shown in Fig. 4 represents a fit of Eq. (9) (i.e., D_{eff}) to our data based on a χ^2 minimization of residuals with the free diffusion coefficient D_0 as the only free parameter. We find $D_0 = 0.140(6)\,m^2/s$, where one-third of the uncertainty in this value arises from the uncertainty in R and the remainder results from the accuracy to which individual values of D_{eff} are measured. This value remains unchanged if the data point acquired with the cell in the rotated position is removed from the fit. Our measurement of D_0 is in agreement with the value $0.136(6)\,m^2/s$ inferred by scaling directly measured values of D for ^{3}He diffusing in ^{4}He reported by Bendt [47] to the conditions of our experiment using the classical high-temperature mass correction factor $\sqrt{8/7}$ [48]. It is also in agreement with the value $D_0 = 0.140(8)\,m^2/s$ obtained by scaling the NMR-based measurement of Barbé et al.[14] [34] to the conditions of our experiment using the temperature dependence of the data reported by Bendt [47]. Careful inspection of our data in the range $\tau \leqslant 4$ ms (i.e., the range where $\ell_d \lesssim \ell_s$) shows that while they are consistent with the fit to Eq. (9), they do lie systematically toward higher values of D_{eff}. A statistical analysis of this bias relative to the remainder of the dataset reveals that Eq. (9) underestimates these particular data by no more than 6% at the 85% confidence level. This is an informative constraint as in principle these data are situated in the intermediate regime for which the gaussian phase approximation (upon which Eq. (9) is based) is not necessarily valid. To the best of our knowledge, this is the only experimental constraint of this nature that has been reported. We also note that the quality of the fit shown in Fig. 4 is not improved by restricting the analysis to diffusion times $\tau > 4$ ms.

A natural question to ask is the extent to which measurements of the time-dependence of spin-echo attenuation factors in the constant gradient limit can provide useful information regarding the dimensionality of a particular restriction. Clearly measurements of spin-echo attenuation factors in the free-diffusion and motionally averaged regimes only determine the product $\beta\ell_s^4$ (cf. Eqs. (1) and (2)). That is, β cannot be determined from such measurements alone without some a priori knowledge of ℓ_s. Conversely, an accurate determination of ℓ_s can only be made if the dimensionality of the restriction and hence β is known.

It is less obvious from a simple inspection of Eqs. (3), (5), and (6) (or equivalently Eqs. (8)–(10)) whether or not measurements of the echo attenuation factor that span the intermediate regime might provide an experimental signature that is sufficient to resolve the dimensionality of a restriction. Examination of Fig. 5, however, suggests that making this type of distinction would be an experimental challenge. The solid curve in Fig. 5 represents the effective diffusion coefficient for an infinite reflecting cylinder (Eq. (9)) of radius R normalized to the effective diffusion coefficient for infinite reflecting planes (Eq. (8)) separated by a distance

$$a' = 2(\beta_2/\beta_1)^{\frac{1}{4}}R = (35/4)^{\frac{1}{4}}R \sim 1.72R \tag{13}$$

and plotted as a function of the measurement period normalized to R^2/D_0. The dashed curve corresponds to the effective diffusion coefficient for an infinite reflecting cylinder of radius R normalized to the effective diffusion coefficient for a reflecting spherical restriction (Eq. (10)) of radius

$$R' = (\beta_2/\beta_3)^{\frac{1}{4}}R = \frac{1}{4}\sqrt{35}/3^{\frac{1}{4}}R \sim 1.12R. \tag{14}$$

The normalization factors appearing in Eqs. (13) and (14) are motivated by the motionally averaged limits of the echo-attenuation factors for each geometry (cf. Eq. (2)). Both of the curves shown in this figure appear to be universal functions that are *independent* of the absolute

[14] The result reported by Barbé et al. was obtained via application of inhomogeneous RF fields rather than pulsed field gradients.

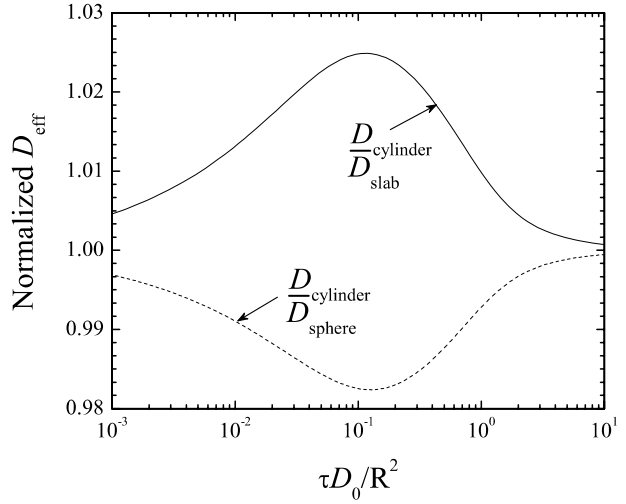

Fig. 5. A comparison of the effective diffusion coefficients for restricted diffusion in one, two, and three dimensions. The spherical and slab geometries result in values of D_{eff} that are maximally different from those produced by the cylindrical geometry for $\ell_d \sim \ell_s/3$. The fact that these differences are so small implies that it would be an experimental challenge to extract detailed information about pore geometry from measurements of D_{eff} alone. On the other hand, it motivates a practical method for scaling effective diffusion coefficients obtained from experiments involving simple one-, two- and three-dimensional restrictions, as outlined in the text.

values of D_0 and R. The time dependence of the effective diffusion coefficient clearly depends upon the dimensionality of the restriction. The above comparison suggests that one-, two-, and three-dimensional restrictions (slab, cylindrical, and spherical geometries, respectively) lead to effective diffusion coefficients that are maximally different for $\ell_d \sim \ell_s/3$. The difference between the values of D_{eff} that one should measure under these conditions, however, is only of order a few percent.

Clearly, without some a priori knowledge of the nature of a restriction, any determination of a structural length-scale ℓ_s from a measurement of the time dependence of D_{eff} in the constant gradient limit is necessarily imprecise. For example, if in our experiment we did not know that the confining volume was a cylinder and we attempted to extract ℓ_s from measurements of D_{eff} using Eq. (8) (one-dimensional restriction or slab geometry) instead of Eq. (9) (two-dimensional restriction or cylindrical geometry) we would have obtained a value that was too small by a factor of $1.72/2 = 0.86$. Likewise if we used Eq. (10) (three-dimensional restriction or spherical geometry) instead of Eq. (9) we would have obtained a value that was too large by a factor of 1.12. Consequently, it is not possible to decide if two pores are truly identical from such data without further information (such as a determination of volume from measurements of an FID amplitude), even if measurements of the time dependence of D_{eff} in both pores are identical.

Finally, the comparison of effective diffusion coefficients shown in Fig. 5 suggests an obvious manner in which data for D_{eff} acquired with the cell axis aligned parallel to the field gradient should be compared to those acquired with the cell axis perpendicular to the field gradient. For *any* value of $D_{\text{eff}}(\tau)$ measured in the slab geometry with plate separation a it is possible to determine an equivalent cylindrical pore of radius R^* cf. Eq. (13) for which Eqs. (8) and (9) yield the same effective diffusion coefficient, to within the small difference specified in Fig. 5. Likewise, it is possible to define an effective diffusion time $\tau^* = \tau(R/R^*)^2$ for which a cylinder of radius R also yields the same value of D_{eff}. This procedure was used to determine the effective diffusion time associated with the data point indicated by the square symbol in Fig. 4.

5. Conclusion

We have used laser optical pumping techniques in conjunction with low pressure ^{3}He gas to demonstrate a novel approach to the study of restricted diffusion within a single well-defined pore. A steady (or constant) gradient-recalled echo sequence was used to characterize diffusion perpendicular to the axis of a cylindrical volume with non-relaxing walls. This measurement can be viewed as the extreme limit of a pulsed gradient diffusion experiment in which the pulse duration is equal to the diffusion time. Measurements were performed over a range of time scales such that the characteristic length scale for diffusion ℓ_d was varied from approximately one-tenth to ten times the characteristic structural length scale ℓ_s of the pore ($\ell_d/\ell_s \sim 0.1$ to $\ell_d/\ell_s \sim 10$). Data for the effective diffusion coefficient D_{eff} spanning more than four decades in magnitude were fit to an analytic solution of the Bloch–Torrey equation based on the gaussian phase approximation. This fit provides a highly constrained value $D_0 = 0.140(6)$ m^2/s for the free-diffusion coefficient of ^{3}He at a temperature and pressure of 296 K and 1.00 Torr, respectively. This value is in excellent agreement with previous results obtained with alternate measurement techniques. The quality of the fit provides useful information, in that the analytic expression for D_{eff} accurately reproduces our data even in the intermediate regime where the validity of the gaussian phase approximation has not been established. It also provides useful insight into the difficulties and limitations associated with attempts to make accurate determinations of pore geometry from studies of restricted diffusion [49–54].

On one hand our experiments simply represent a two-dimensional analogue to the pioneering experiments of Wayne and Cotts [12]; differences between the two experiments are purely geometric. On the other hand we have been able to circumvent and/or eliminate facets of

the original work that today might be considered problematic. With the advantage of hindsight, for example, it is evident that Wayne and Cotts' explored a range of parameter space that ventured into the localization regime rather than the desired motional-averaging regime [14]. Our data avoid the localization regime altogether and venture much further into the motional-averaging regime. At the same time, through a novel approach to cell construction and the use of very low magnetic fields, we have effectively eliminated concerns that might arise from wall-induced nuclear relaxation. Finally, through the use of low-pressure gas with a correspondingly large diffusion coefficient we have been able to work in a regime where pore geometry can be controlled and characterized to a high degree of accuracy. This aspect of our experiment holds considerable promise for future investigation, particularly in the study of pores with complex geometries.

Acknowledgments

We are grateful to M.D. Hürlimann and C.P. Bidinosti for their critical reading of this manuscript. This work was supported by the Natural Sciences and Engineering Research Council of Canada and the British Columbia Advanced Systems Institute.

References

[1] E.L. Hahn, Spin echoes, Phys. Rev. 80 (1950) 580–594.
[2] H.Y. Carr, E.M. Purcell, Effects of diffusion on free precession in nuclear magnetic resonance experiments, Phys. Rev. 94 (1954) 630–638.
[3] S. Meiboom, D. Gill, Modified spin-echo method for measuring nuclear relaxation times, Rev. Sci. Intrum. 29 (1958) 688–691.
[4] E.O. Stejskal, J.E. Tanner, Spin diffusion measurements: spin echoes in the presence of a time-dependent field gradient, J. Chem. Phys. 42 (1965) 288–292.
[5] R.M. Cotts, M.J.R. Hoch, T. Sun, J.T. Marker, Pulsed field gradient stimulated echo methods for improved NMR diffusion measurements in heterogeneous systems, J. Magn. Reson. 83 (1989) 252–266.
[6] P.J. Basser, J. Mattiello, D. LeBihan, MR diffusion tensor spectroscopy and imaging, Biophys. J. 66 (1994) 259–267.
[7] J.R. Mayo, M.E. Hayden, Hyperpolarized Helium 3 diffusion imaging of the lung, Radiology 222 (2002) 8–11, and references therein.
[8] M.D. Hürlimann, K.G. Helmer, L.L. Latour, C.H. Sotak, Restricted diffusion in sedimentary rocks. Determination of surface-area-to-volume ratio and surface relaxivity, J. Magn. Reson. A 111 (1994) 169–178.
[9] P.T. Callaghan, Principles of Nuclear Magnetic Resonance Microscopy, Oxford University Press, New York, 1991.
[10] R.W. Mair, G.P. Wong, D. Hoffmann, M.D. Hürlimann, S. Patz, L.M. Schwartz, R.L. Walsworth, Probing porous media with gas diffusion NMR, Phys. Rev. Lett. 83 (1999) 3324–3327.
[11] R. Kimmich, NMR Tomography, Diffusometry, Relaxometry, Springer-Verlag, New York, 1997.
[12] R.C. Wayne, R.M. Cotts, Nuclear-magnetic-resonance study of self-diffusion in a bounded medium, Phys. Rev. 151 (1966) 264–272;
Erratum, Phys. Rev. 159 (1967) 486.
[13] K.G. Helmer, M.D. Hürlimann, T.M. de Swiet, P. Sen, C.H. Sotak, Determination of ratio of surface area to pore volume from restricted diffusion in a constant field gradient, J. Magn. Reson. A 115 (1995) 257–259.
[14] M.D. Hürlimann, K.G. Helmer, T.M. de Swiet, P.N. Sen, C.H. Sotak, Spin echoes in a constant gradient and in the presence of simple restriction, J. Magn. Reson. A 113 (1995) 260–264.
[15] M. Appel, G. Fleischer, D. Geschke, J. Kärger, M. Winkler, Pulsed-field-gradient NMR analogue of the single-slit diffraction pattern, J. Magn. Reson. A 122 (1996) 248–250.
[16] A. Coy, P.T. Callaghan, Pulsed gradient spin echo nuclear magnetic resonance for molecules diffusing between partially reflecting rectangular barriers, J. Chem. Phys. 101 (1994) 4599–4609.
[17] D. Topgard, O. Söderman, Experimental determination of pore shape and size using q-space NMR microscopy in the long diffusion-time limit, Magn. Reson. Imaging 21 (2003) 69–76.
[18] W.S. Price, P. Stilbs, O. Söderman, Determination of pore space shape and size in porous systems using NMR diffusometry. Beyond the short gradient pulse approximation, J. Magn. Reson. 160 (2003) 139–143.
[19] S.J. Gibbs, Observations of diffusive diffraction in a cylindrical pore by PFG NMR, J. Magn. Reson. 124 (1996) 223–226.
[20] C.H. Neuman, Spin echo of spins diffusing in a bounded medium, J. Chem. Phys. 60 (1974) 4508–4511.
[21] P. Linse, O. Söderman, The validity of the short-gradient-pulse approximation in NMR studies of restricted diffusion. Simulations of molecules diffusing between planes, in cylinders and spheres, J. Magn. Reson. A 116 (1995) 77–86.
[22] P.T. Callaghan, A simple matrix formalism for spin echo analysis of restricted diffusion under generalized gradient waveforms, J. Magn. Reson. 129 (1997) 74–84.
[23] S.L. Codd, P.T. Callaghan, Spin echo analysis of restricted diffusion under generalized gradient waveforms: planar, cylindrical, and spherical pores with wall relaxivity, J. Magn. Reson. 137 (1999) 358–372.
[24] D.E. Woessner, NMR spin-echo self-diffusion measurements on fluids undergoing restricted diffusion, J. Phys. Chem. 67 (1963) 1365–1367.
[25] H.C. Torrey, Bloch equations with diffusion terms, Phys. Rev. 104 (1956) 563–565.
[26] A. Abragam, The Principles of Nuclear Magnetism, Oxford University Press, New York, 1986.
[27] B. Robertson, Spin-echo decay of spins diffusing in a bounded region, Phys. Rev. 151 (1966) 273–277.
[28] R.M.E. Valkenborg, H.P. Huinink, J.J.v.d. Sande, K. Kopinga, Random-walk simulations of NMR dephasing effects due to uniform magnetic field gradients in a pore, Phys. Rev. E 65 (2002) 021306–021313.
[29] D.C. Douglass, D.W. McCall, Diffusion in paraffin hydrocarbons, J. Phys. Chem. 62 (1958) 1102–1107.
[30] T.M. de Swiet, P.N. Sen, Decay of nuclear magnetization by bounded diffusion in a constant field gradient, J. Chem. Phys 100 (1994) 5597–5604.
[31] J.C. Tarczon, W.P. Halperin, Interpretation of NMR diffusion measurements in uniform- and nonuniform-field profiles, Phys. Rev. B 32 (1985) 2798–2807.
[32] B. Balinov, B. Jönsson, P. Linse, O. Söderman, The NMR self-diffusion method applied to restricted diffusion. Simulation of echo attenuation from molecules in spheres and between planes, J. Magn. Reson. A 104 (1993) 17–25.
[33] S.D. Stoller, W. Happer, F.J. Dyson, Transverse spin relaxation in inhomogeneous magnetic fields, Phys. Rev. A 44 (1991) 7459–7477.

[34] R. Barbé, M. Leduc, F. Lalöe, Résonance magnétique en champ de radiofréquence inhomogène 1re partie: Études théorique, J. Phys. 35 (1974) 699–725.
[35] G.D. Cates, S.R. Schaefer, W. Happer, Relaxation of spins due to field inhomogeneities in gaseous samples at low magnetic fields and low pressures, Phys. Rev. A 37 (1988) 2877–2885.
[36] C.L. Bohler, D.D. McGregor, Transverse relaxation in spin-polarized ^{3}He gas due to dc and ac magnetic-field gradients, Phys. Rev A 49 (1995) 2755–2758.
[37] D.D. McGregor, Transverse relaxation of spin-polarized ^{3}He gas due to a magnetic field gradient, Phys. Rev. A 41 (1990) 2631–2635.
[38] R. Barbé, M. Leduc, F. Lalöe, Résonance magnétique en champ de radiofréquence inhomogène 2e partie: vérifications expérimentales; mesure du coefficient de self-diffusion de ^{3}He, J. Phys. 35 (1974) 935–951.
[39] G.D. Cates, D.J. White, T.-R. Chien, S.R. Schaefer, W. Happer, Spin relaxation in gases due to inhomogeneous static and oscillating magnetic fields, Phys. Rev. A 38 (1988) 5092–5106.
[40] Shott Duran 8330.
[41] M&I Materials Ltd, UK.
[42] B. Saam, W. Happer, H. Middleton, Nuclear relaxation of ^{3}He in the presence of O_2, Phys. Rev. A 52 (1995) 862–865.
[43] J.G. Ganière, Relaxation nucléaire de ^{3}He gazeux par des surfaces, Helv. Phys. Acta 46 (1973) 147.
[44] F.D. Colegrove, L.D. Schearer, G.K. Walters, Polarization of ^{3}He gas by optical pumping, Phys. Rev. 132 (1963) 2561–2572.
[45] E.M. Purcell, Helmholtz coils revised, Am. J. Phys. 57 (1989) 18–22.
[46] J.L. Hobson, C.P. Bidinosti, K.M. Gilbert, C. Lei, G. Archibald, M.E. Hayden, Breakdown of the high-field approximation in the context of hyperpolarized ^{3}He MRI, Proc. Intl. Soc. Mag. Reson. Med. 12 (2004) 1679.
[47] P.J. Bendt, Measurements of ^{3}He–^{4}He and H_2–D_2 gas diffusion Coefficients, Phys. Rev. 110 (1958) 85–89.
[48] J.O. Hirschfelder, C.F. Curtiss, R.B. Bird, Molecular Theory of Gases and Liquids, Wiley, New York, 1954.
[49] R.L. Kleinberg, M.A. Horsefield, Transverse relaxation processes in porous sedimentary rock, J. Magn. Reson. 88 (1990) 9–19.
[50] X. Josette Chen, H.E. Möller, M.S. Chawla, G.P. Cofer, B. Driehuys, L.W. Hedlund, G.A. Johnson, Spatially resolved measurements of hyperpolarized gas properties in the lung in vivo. Part I: diffusion coefficient, Magn. Reson. Med. 42 (1999) 721–728.
[51] X. Josette Chen, L.W. Hedlund, H.E. Möller, M.S. Chawla, R.R. Marɔnpot, G.A. Johnson, Detection of emphysema in rat lungs by using magnetic resonance measurements of ^{3}He diffusion, PNAS 97 (2000) 11478–11481.
[52] B.T. Saam, D.A. Yablonskiy, V.D. Kodibagkar, J.C. Leawoods, D.S. Gierada, J.D. Cooper, S.S. Lefrak, M.S. Conradi, MR imaging of diffusion of ^{3}He gas in healthy and diseased lungs, Magn. Reson. Med. 44 (2000) 174–179.
[53] D.A. Yablonskiy, A.L. Sukstanskii, J.C. Leawoods, D.S. Gierada, G.L. Bretthorst, S.S. Lefrak, J.D. Cooper, M.S. Conradi, Quantitative in vivo assessment of lung microstructure at the alveolar level with hyperpolarized ^{3}He diffusion MRI, PNAS 99 (2002) 3111–3116.
[54] S. Fichele, M.N.J. Paley, N. Woodhouse, P.D. Griffiths, E.J.R. van Beek, J.M. Wild, Investigating ^{3}He diffusion NMR in the lungs using finite difference simulations and in vivo PGSE experiments, J. Magn. Reson. 167 (2004) 1–11.